



Simulation and Optimization of Lead-Based Perovskite Solar Cells with Cuprous Oxide as a P-type Inorganic Layer

D. Eli^{a,d,*}, M. Y. Onimisi^a, S. Garba^b, R. U. Ugbe^a, J. A. Owolabi^a, O. O. Ige^a, G. J. Ibeh^a, A. O. Muhammed^c

^aDepartment of Physics, Nigerian Defence Academy, Kaduna, Nigeria

^bDepartment of Chemistry, Nigerian Defence Academy, Kaduna, Nigeria

^cDepartment of Physics, Bayero University, Kano, Nigeria

^dDepartment of Physical Sciences, Greenfield University, Kaduna, Nigeria

Abstract

The hole transporting material (HTM) is responsible for selectively transporting holes and blocking electrons which also plays a crucial role in the efficiency and stability of perovskite solar cells (PSCs). Spiro-MeOTAD is the most popular material, which is expensive and can be easily affected by moisture contents. There is need to find an alternative HTM with sufficiently high resistance to moisture content. In this paper, the influence of some parameters with cuprous oxide (Cu_2O) as HTM was investigated using solar cell capacitance simulator (SCAPS). These include the influence of doping concentration and thickness of absorber layer, the effect of thickness of ETM and HTM as well as electron affinities of ETM and HTM on the performance of the PSCs. From the obtained results, it was found that concentration of dopant in absorber layer, thickness of ETM and HTM and the electron affinity of HTM and ETM affect the performance of the solar cell. The cell performance improves greatly with the reduction of ETM electron affinity and its thickness. Upon optimization of parameters, power conversion efficiency for this device was found to be 20.42 % with current density of 22.26 mAcm^{-2} , voltage of 1.12 V, and fill factor of 82.20 %. The optimized device demonstrates an enhancement of 58.80 %, 2.25 %, 20.40 % and 30.23 % in PCE, Jsc, FF and Voc over the initial cell. The results show that Cu_2O in lead-based PSC as HTM is an efficient system and an alternative to spiro-MeOTAD.

Keywords: Perovskite solar cells, inorganic HTM, device simulation, cuprous oxide, defect density

Article History :

Received: 26 April 2019

Received in revised form: 16 May 2019

Accepted for publication: 18 May 2019

Published: 30 August 2019

©2019 Journal of the Nigerian Society of Physical Sciences. All rights reserved.
Communicated by: B. J. Falaye

1. Introduction

The exciting properties, including tuned band gap, small exciton energy, excellent bipolar carrier transport, long charge diffusion, and amazingly high tolerance to defects [1-7], perovskite halides have demonstrated promising abilities for a numerous of optoelectronic applications, including photovoltaics,

light-emission, photodetectors, x-rays imaging, lasers, gamma ray detection etc [8-14].

Perovskite solar cells (PSCs) based on lead have demonstrated remarkable breakthrough in almost a decade since after its invention due to its advantages of low cost, high efficiency and simple fabrication process. Its efficiency has grown from 3.9 % in 2009 to over 23 % in late 2018 [16, 17]. Despite its remarkable attainment, these power conversion efficiencies are still low as compared to inorganic solar cells such as crystalline silicon (*c-Si*, 25.7 %), gallium arsenide (*GaAs*, 28.8 %)

*Corresponding author tel. no: +2348063307256

Email address: danladielibako@gmail.com (D. Eli)

etc [18]. Methyl ammonium lead iodide ($\text{CH}_3\text{NH}_3\text{PbI}_3$) with a band gap of 1.50 eV that covers absorption within wide range of visible spectrum was reported by various experimental and theoretical studies [18, 19]. Generally, PSC is made up of hole transporting layer, electron transporting layer and absorber layer. The function demonstrated by each layer in PSC should be understood in order to enhance the performance of the device [20].

The most routinely used electron transporting material (ETM) is TiO_2 because of its suitable energy level for electron injection, high electron mobility, good stability and environmental friendliness [3, 4, 7, 18]. It is often a difficult task to make good choice of hole transporting materials which are needed for extracting holes effectively from the perovskite layer while preventing electrons from recombination.

The most commonly used hole transport material is Spiro-OMeTAD which is organic in nature [21]. It is made up of basically two additives, 4-tert-butylpyridine (TBP) and bis (trifluoromethane) sulfonamide lithium salt (Li-TFSI), which are used to improve the conductivity and hole mobility of spiro-MeOTAD. The most commonly used HTM demonstrate hygroscopic nature, tendency to crystalize, and vulnerability to both moisture and heat, as such must be replaced with a cost effective and stable HTM having high hole mobility with ease of synthesis [18, 22, 23, 24].

Robust metal oxide [25, 26], carbon [27, 28], and other inorganic materials [18, 29] have shown outstanding behaviours in stabilizing the device, but in the meantime, the optimization of PCE in these devices is still necessary for accelerating the commercialization. Inorganic p-type semi-conductor such as Cu_2O is considered to be an alternative to organic HTMs [30].

PCE has been greatly enhanced and reached up to 11.03 % when Cu_2O film was prepared via a facile process of Cu sputtering and controlled thermal oxidation [30, 31]. Except for experimental work, it is also equally important to investigate all aspects of the device theoretically in order to fully understand the device mechanism and optimize the device performance.

Considering Cu_2O as HTM in lead based PSCs, very few works have been demonstrated so far. For example, perovskite ($\text{CH}_3\text{NH}_3\text{PbI}_3$) solar cells with Cu_2O as HTM was simulated using SCAPS, while only the effect of thickness of the absorber on the performance of PSCs was investigated [32, 33]. A device model that involve the simulation of various HTMs with Cu_2O inclusive, was done but with no sufficient investigation on various parameters (only thickness of absorber) was carried out [34].

In addition to the thickness of the absorber, there are also many other important parameters which could affect the performance of PSCs. These include doping concentration in the absorber layer, thickness of the ETM and electron affinity of ETM and HTM. For example, proper choice of suitable electron affinity of ETM and HTM can prevent exciton quenching at the interface, thus can assist in enhancing device performance. As such, a comprehensive study of these parameters needs to be investigated in order to uncover further understanding and thus improve device performance. In this paper, simulation of lead based $\text{CH}_3\text{NH}_3\text{PbI}_3$ PSCs with Cu_2O as HTM and TiO_2 as ETM was done with SCAPS. The influence of all above men-

tioned parameters on the performance of PSCs were studied systematically.

2. Device Simulation Parameters

The structure of our simulated PSC is considered with layer configuration of glass substrate/TCO (transparent conducting oxide)/ TiO_2 (ETM) absorber layer $\text{CH}_3\text{NH}_3\text{PbI}_3/\text{Cu}_2\text{O}$ (HTM)/metal back contact. The structure and the band diagram is shown in figure 1 (a) and (b). From the band structure, the valence band offset at the $\text{CH}_3\text{NH}_3\text{PbI}_3/\text{Cu}_2\text{O}$ interface is +0.08 eV, which can be considered beneficial for the flow of holes to the back-metal contact in order to avoid their recombination with the electrons in the perovskite layer.

The conduction band offset is +0.30 eV at the $\text{TiO}_2/\text{CH}_3\text{NH}_3\text{PbI}_3$ interface, which is also necessary for the flow of photo excited electrons to the front electrode. Neutral Gaussian distribution defect is selected in the absorber layer and characteristic energy is set to be 0.1 eV [18]. Two defect interfaces are inserted for carrier recombination. One defect interface is $\text{TiO}_2/\text{CH}_3\text{NH}_3\text{PbI}_3$ and the other one is $\text{CH}_3\text{NH}_3\text{PbI}_3/\text{Cu}_2\text{O}$.

The nature of the defect is set as Gaussian and defect density is set as $1 \times 10^{18} \text{ cm}^{-3}$ [18, 32]. Table 1 shows the defect parameters which are used in the simulation. Basic parameters for each material used in the simulation are summarized in Table 2. Thermal velocities of hole and electron are selected as 107 cm s^{-1} [18, 32, 35, 36]. The optical reflectance is considered to be zero at the surface and at each interface [18]. Parameters are optimized in the study by using control variable method. The initial total defect density of the absorber layer is assumed to be $2.5 \times 10^{13} \text{ cm}^{-3}$.

The current density–voltage curve has been drawn with these initial parameters as shown in Figure 2(A).

The short-circuit current density (J_{sc}) of 21.77 mA cm^{-2} , open-circuit voltage (V_{oc}) of 0.865 V, Fill Factor (FF) of 68.27 %, and PCE of 12.86 % are obtained. The simulated device performance is consistent with the experimental results of lead-based PSCs [30, 31]. This consistency shows that input parameters are valid and close to the real device. In the incident photon-to-current efficiency (IPCE) of the device shown in figure 2(B) which is featured with a high platform between 300 nm and 850 nm with the maximum of 90 % at 570 nm. Optical absorption edge is red shifted to 800 nm which corresponds to a band gap of 1.55 eV in $\text{CH}_3\text{NH}_3\text{PbI}_3$. The IPCE covers the whole visible spectrum which is closer to the experimental work [30, 31].

3. Results and Discussion

3.1. Influence of doping concentration (N_A) of absorber layer

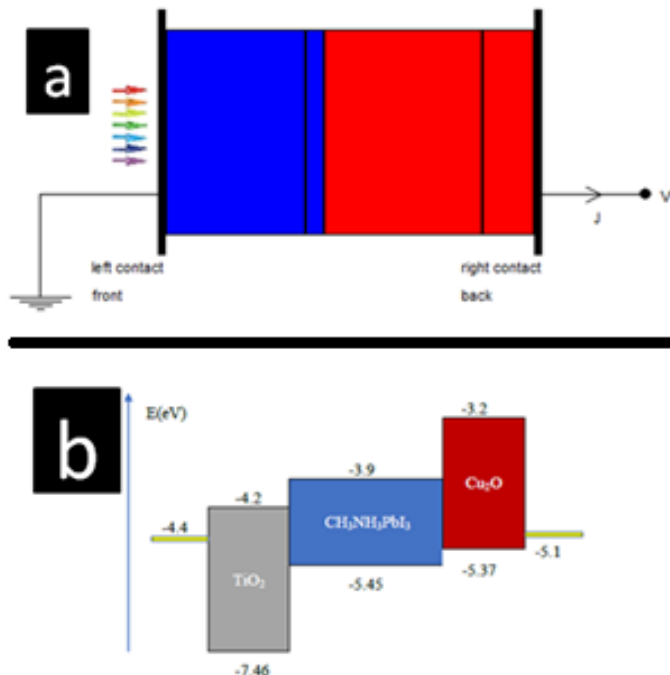
In order to enhance the performance of solar cells, doping is a key process considered. Depending upon the type of dopants, doping can either be n-type or p-type. Like the other crystalline semiconductors, the shallow point defects in absorber could cause unintentional doping at room temperature. The performance of PSC can be enhanced by introducing appropriate

Table 1: Defect parameters of interfaces and absorber [18, 32]

Parameters	$CH_3NH_3PbI_3$	$TiO_2/CH_3NH_3PbI_3$ interface	$CH_3NH_3PbI_3/Cu_2O$ interface
Defect type	Neutral	Neutral	Neutral
Capture cross section for electrons (cm^2)	2×10^{-15}	2×10^{-16}	2×10^{-15}
Capture cross section for holes (cm^2)	2×10^{-15}	2×10^{-16}	2×10^{-15}
Energetic distribution	Gaussian	Single	Single
Energetic level with respect to $E_v(eV)$	0.500	0.650	0.650
Characteristic energy (eV)	0.1	0.1	0.1
Total density (cm^{-3})	$1 \times 10^{15} - 1 \times 10^{19}$	1×10^{18}	1×10^{18}

Table 2: Simulation parameters of PSCs devices

Parameters	FTO	ETM (TiO_2)	Absorber	HTM (Cu_2O)
Thickness (μm)	0.4	0.05	0.45	0.15
Band gap energy E_g (eV)	3.5	3.26 [32]	1.55[32]	2.17[32]
Electron affinity $\chi(eV)$	4.0	4.2[32]	3.9[18]	3.2[32]
Relative permittivity ϵ_r	9	10	6.5	7.11[32]
Effective conduction band density $N_c(cm^{-3})$	2.2×10^{18}	2.2×10^{18} [32]	2.2×10^{18} [32]	2.2×10^{18} [32]
Effective valance band density $N_v(cm^{-3})$	2.2×10^{18}	2.2×10^{18} [32]	2.2×10^{18} [32]	2.2×10^{18} [32]
Electron mobility $\mu_n(cm^2V^{-1}s^{-1})$	20	20[18, 32]	2[32, 33]	80[32, 39]
Hole mobility $\mu_p(cm^2V^{-1}s^{-1})$	10	10[18, 32]	2[32, 33]	80[32, 39]
Donor concentration N_D (cm^{-3})	1×10^{19}	1×10^{17}	0	0
Acceptor concentration N_A (cm^{-3})	0	0	1×10^{13} [7, 32]	1×10^{18} [18, 32]
Defect density N_t (cm^{-3})	1×10^{15}	1×10^{15} [18, 32]	2.5×10^{13} [18, 32]	1×10^{15} [18, 32]

Figure 1: (a) The structure of perovskite solar cell in the simulation and (b) Energy level diagram of Cu_2O in the device

dopant in absorber layer [18, 37]. The self-doping process can be adopted for n- or p-type doping in absorber layer. It has been demonstrated experimentally that n-type or p-type self-doping in $CH_3NH_3PbI_3$ lead towards the manipulation of carrier density, majority carrier type and charge transport by changing the

thermal annealing or precursor ratios in the solutions [37, 38].

Formation of $CH_3NH_3PbI_3$ involves organic and inorganic precursors named methyl ammonium iodide (MAI) and lead iodide (PbI_2). The ratio between precursors (PbI_2/MAI) decides the doping of the absorber. Upon thermal annealing, PbI_2 rich absorber layer is n-doped and PbI_2 deficit absorber layer is p-doped [39]. Furthermore, $CH_3NH_3PbI_3$ is unstable in air and humidity.

When moist air comes in contact with device then PbI_2 is generated and oxidation state of lead is changed. This process is the cause of introducing impurities in absorber layer. The effect of doping concentration on the performance of perovskite solar cell is studied by choosing the values of N_A in the range of 10^{14} – $10^{17} cm^{-3}$. Table 3 gives the PCE of PSC with various values of doping concentration. It is worth noting that PCE is maximum when the value of N_A is $1 \times 10^{15} cm^{-3}$. J_{sc} also has the same behaviour. The results above demonstrate that charge carriers are transported and collected more efficiently at the same irradiance when N_A of the absorber is $1 \times 10^{15} cm^{-3}$.

Therefore, proper selection of N_A is necessary for the improvement of performance of PSCs. On the other hand, J_{sc} and V_{oc} decrease when values of N_A increases beyond $1 \times 10^{15} cm^{-3}$. The variation in the cell performance with the doping concentration can be explained in terms of built-in electric field which is enhanced with the increase of doping concentration. The charge carriers are separated and increased by the increase of electric field resulting in the enhanced performance of PSCs [18, 40].

The decrease in J_{sc} with increasing doping concentration could be explained from the perspective of Auger recombina-

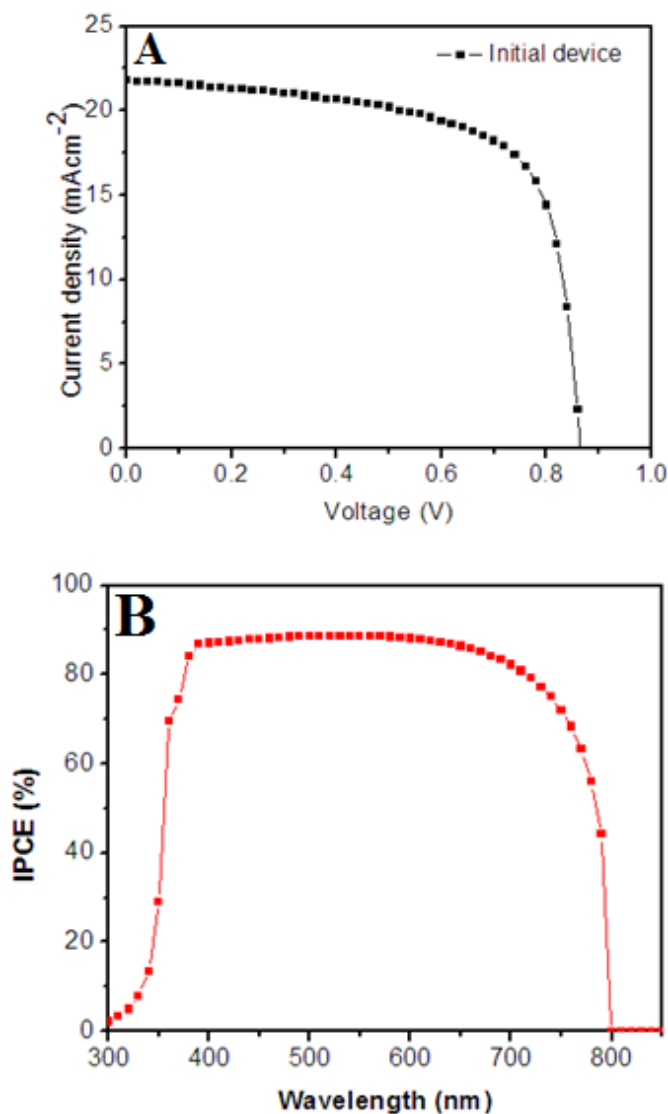


Figure 2: (A) J–V curve of PSC with initial parameters, (B) IPCE spectra of the device with initial parameters

tion. Auger recombination rate increases with further increase of doping density beyond $1 \times 10^{15} \text{ cm}^{-3}$. It is also clear that total recombination rate also increases when doping density increases beyond $1 \times 10^{15} \text{ cm}^{-3}$. The scattering and recombination increases due to increasing doping density thus suppressing hole transportation [18, 41]. Therefore, optimum doping density enhances the Voc and Jsc which in turn increases the PCE. While further increase in doping density is not favourable due to high recombination and scattering.

There should be lower carrier concentration in lead perovskite so that carrier mobility can increase within the absorber. The optimum performance with Jsc of 22.10 mAcm^{-2} , Voc of 0.85 V , FF of 73.97% and PCE of 13.82% is obtained under the doping density of $1 \times 10^{15} \text{ cm}^{-3}$. The comparison is shown between J–V curves with different value of N_A in Figure 3(B). With the optimization, PCE was enhanced by 7.38% , and Jsc increases 1.52% , as compared with the device having initial

value of $N_A = 1 \times 10^{13} \text{ cm}^{-3}$. Figure 3(A) shows the simulation results by changing the value of doping concentration from 1×10^{15} to $1 \times 10^{17} \text{ cm}^{-3}$ with respect to photovoltaic parameters (PCE, Voc, Jsc, and FF).

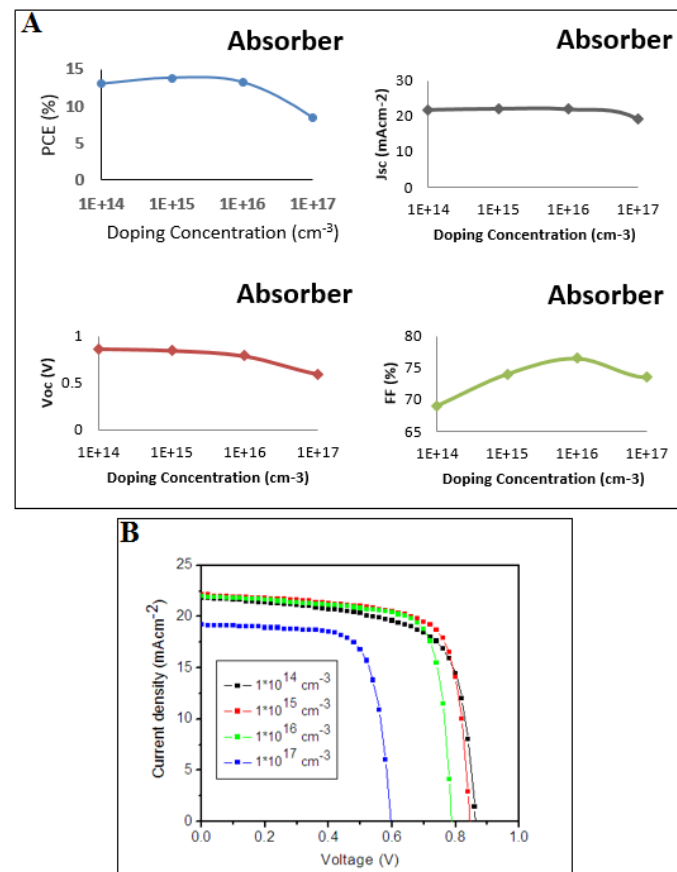


Figure 3: (A) Variation in performance parameters of PSC with doping concentration of absorber, (B) J–V curves of PSC with different values of doping concentration.

3.2. Influence of electron affinity of ETM and HTM

One of the important factor considered in TiO_2 /perovskite/ Cu_2O is band offset which becomes a determining factor as to the carrier recombination at the interface and is the measure of Voc. By varying the values of electron affinities of TiO_2 ($3.7\text{--}4.3 \text{ eV}$) and Cu_2O ($3.1\text{--}3.7 \text{ eV}$), the band offset can be adjusted. Figures 4(A) and 5(A) show variation of PCE, Voc, Jsc and FF with electron affinity of ETM and HTM respectively. The values of 3.7 eV and 3.3 eV give the best PCE for TiO_2 and Cu_2O respectively. When the electron affinity of ETM is high (greater than 3.7 eV), then Voc and Jsc decrease slightly. PCE of 20.29% , Jsc of 22.55 mAcm^{-2} , Voc of 1.10 V and FF of 81.72% were obtained upon optimizing value of electron affinity of ETM, as shown in Table 4 and PCE of 13.11% , Jsc of 21.87 mAcm^{-2} , Voc of 0.87 V and FF of 69.31% were obtained upon optimizing value of electron affinity of HTM, as shown in Table 5. It is evident that proper ETM and HTM selection with suitable electron affinity can reduce the recombination of car-

Table 3: Dependence of solar cell performance on the doping concentration of Absorber layer

Parameters	$N_A(cm^{-3})$	$J_{sc}(mAcm^{-2})$	$V_{oc} (V)$	FF	PCE (%)
10^{14}		21.80	0.86	69.02	12.99
10^{15}		22.80	0.85	73.97	13.82
10^{16}		21.96	0.79	76.43	13.21
10^{17}		19.20	0.60	73.45	8.40

riers and performance of PSCs can further be optimised [42].

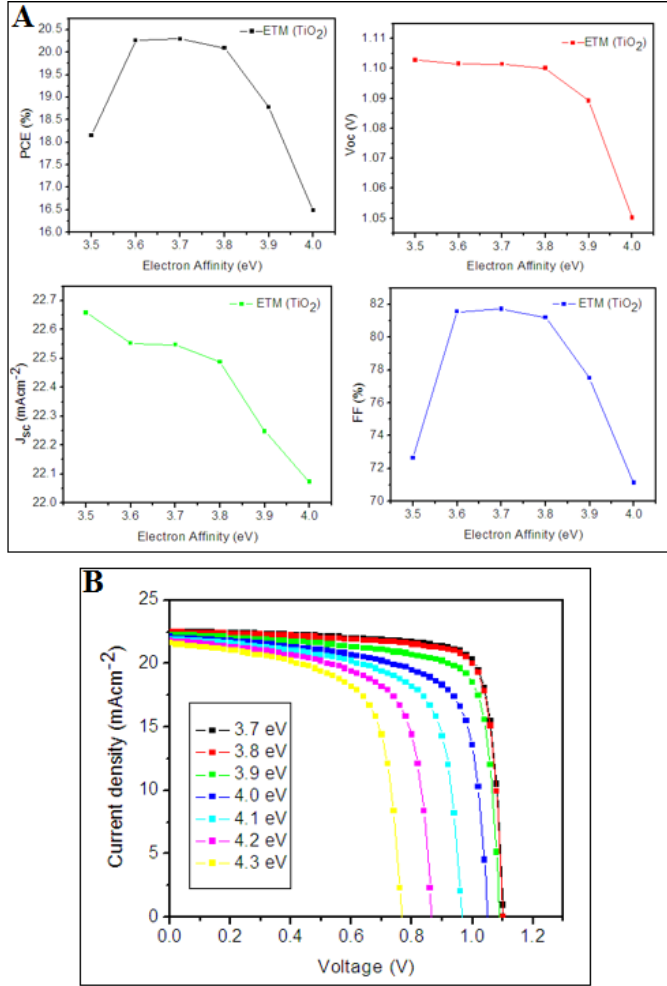


Figure 4: (A) Variation in performance parameters of PSC with electron affinity of ETM, (B) J–V curves of PSC with different values of electron affinity of ETM.

3.3. Influence of thickness of ETM and HTM

Figure 6(A) is the plot of solar cell parameters; V_{OC} , J_{SC} , FF and PCE versus thickness of the ETM; TiO_2 . In both cases V_{OC} , J_{SC} , FF and PCE are gradually decreasing due to fractional absorption of incident light by the TiO_2 layer, the bulk recombination and surface recombination at the interface [15]. Thickness of ETMs has been varied from 0.001 to 0.160 μm which shows a decrease in photovoltaic parameters with increase in ETM thickness, as shown in Table 6. Similarly, Fig-

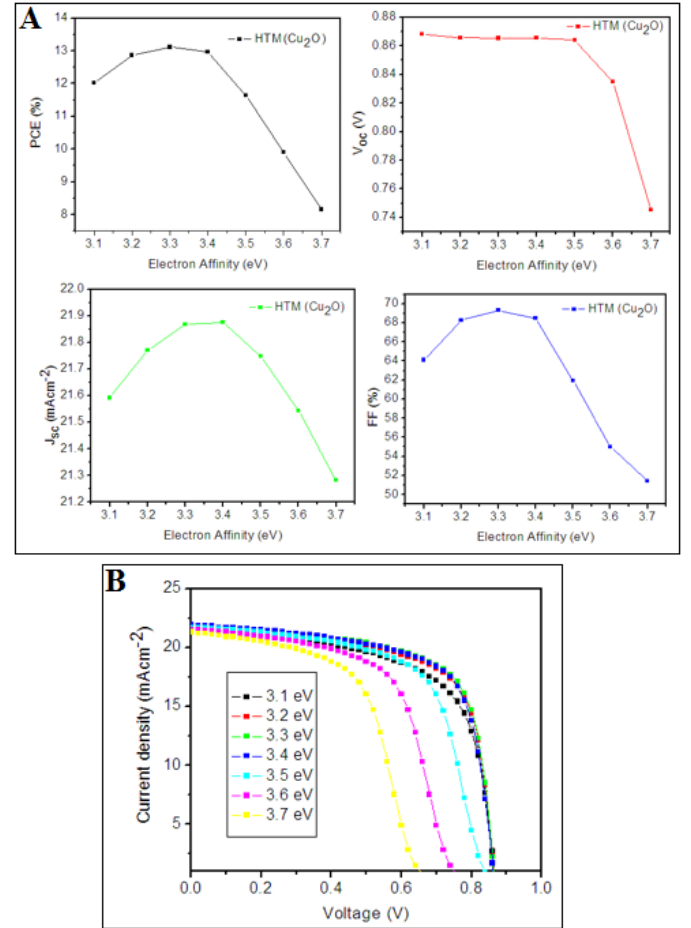


Figure 5: (A) Variation in performance parameters of PSC with electron affinity of HTM, (B) J–V curves of PSC with different values of electron affinity of HTM.

ure 6(B) shows reverse case as V_{OC} , J_{SC} , FF and PCE increase with increase in HTM up to 0.02 μm . Above 0.02 μm we noticed a constant value for V_{OC} , J_{SC} , FF and PCE, which means the thickness that gives optimum performance is from 0.04 to 0.16 μm . The slightly increase with increase in thickness up to 0.02 μm suggests the higher conductivity of the TiO_2 and partial absorption of the light. PCE of 15.52 %, J_{sc} of 22.10 $mAcm^{-2}$, V_{OC} of 1.01 V and FF of 69.81 % are obtained at a thickness of 0.001 μm which is the optimized value of HTM thickness and PCE of 12.87 %, J_{SC} of 21.77 $mAcm^{-2}$, V_{OC} of 0.87 V and FF of 68.27 % are obtained, as shown in Table 7.

Table 4: Dependence of solar cell performance on the electron affinity of ETM

Parameters	$EA(eV)$	$Jsc(mAcm^{-2})$	$Voc(V)$	FF	PCE (%)
3.7		22.50	1.10	81.72	20.29
3.8		22.49	1.10	81.20	20.10
3.9		22.25	1.09	77.50	18.78
4.0		22.07	1.05	71.14	16.49
4.1		21.93	0.97	69.21	14.64
4.2		21.77	0.87	68.27	12.87
4.3		21.58	0.77	67.36	11.13

Table 5: Dependence of solar cell performance on the HTM

Parameters	$EA(eV)$	$Jsc(mAcm^{-2})$	$Voc(V)$	FF	PCE (%)
3.1		21.59	0.87	64.10	12.01
3.2		21.77	0.87	68.27	12.87
3.3		21.87	0.87	69.31	13.11
3.4		21.88	0.87	68.48	12.96
3.5		21.74	0.86	61.94	11.64
3.6		21.54	0.83	55.03	9.90
3.7		21.28	0.75	51.43	8.16

Table 6: Dependence of solar cell performance on the ETM

Parameters	$T(\mu m)$	$Jsc(mAcm^{-2})$	$Voc(V)$	FF	PCE (%)
0.0010		22.10	1.01	69.81	15.52
0.0025		22.05	0.97	69.37	14.89
0.0050		22.00	0.95	69.12	14.37
0.0100		21.93	0.91	69.84	13.81
0.0200		21.86	0.89	68.50	13.27
0.0400		21.79	0.87	68.33	12.93
0.0800		21.73	0.86	68.27	12.81
0.1600		21.64	0.86	68.30	12.76

Table 7: Dependence of solar cell performance on the HTM

Parameters	$T(\mu m)$	$Jsc(mAcm^{-2})$	$Voc(V)$	FF	PCE (%)
0.0010		21.23	0.82	55.61	9.66
0.0025		21.24	0.82	55.73	9.76
0.0050		21.29	0.84	56.41	10.12
0.0100		21.51	0.87	62.00	11.58
0.0200		21.76	0.87	68.15	12.84
0.0400		21.77	0.87	68.27	12.87
0.0800		21.77	0.87	68.27	12.87
0.1600		21.77	0.87	68.27	12.87

Table 8: Dependence of solar cell performance on the Absorber

Parameters	$T(\mu m)$	$Jsc(mAcm^{-2})$	$Voc(V)$	FF	PCE (%)
0.2		17.57	0.83	74.16	10.78
0.3		20.32	0.85	71.75	12.32
0.4		21.43	0.86	69.51	12.83
0.5		21.99	0.87	67.05	12.82
0.6		22.20	0.87	64.72	12.52
0.7		22.21	0.88	62.50	12.22
0.8		22.10	0.88	60.48	11.82
0.9		21.93	0.87	58.67	11.41

Table 9: Optimized Parameters of the device

Optimized parameters	ETM(TiO_2)	Absorber ($CH_3NH_3PbI_3$)	HTM(Cu_2O)
Doping density (cm^{-3})	–	1×10^{15}	–
Electron affinity (eV)	3.7	–	3.3
Thickness (μm)	0.0010	0.4000	0.1600

Table 10: Photovoltaic parameters of Cu_2O based perovskite solar cells reported in the experimental work in the literature and simulated results using SCAPS.

Simulation	$J_{sc}(mAcm^{-2})$	$V_{oc}(V)$	FF	PCE (%)
Initial	21.76	0.86	68.26	12.86
Optimized N_A of absorber	22.09	0.85	73.97	13.82
Optimized thickness of absorber	21.43	0.86	69.51	12.83
Optimized EA of ETM	22.55	1.10	81.72	20.29
Optimized EA of HTM	21.87	0.87	69.31	13.11
Optimized thickness of ETM	22.10	1.00	69.81	15.52
Optimized thickness of HTM	21.77	0.87	68.27	12.87
Final optimization	22.26	1.12	82.20	20.42
[30]	17.50	0.95	66.20	11.03
[31]	19.02	0.99	73.63	13.97

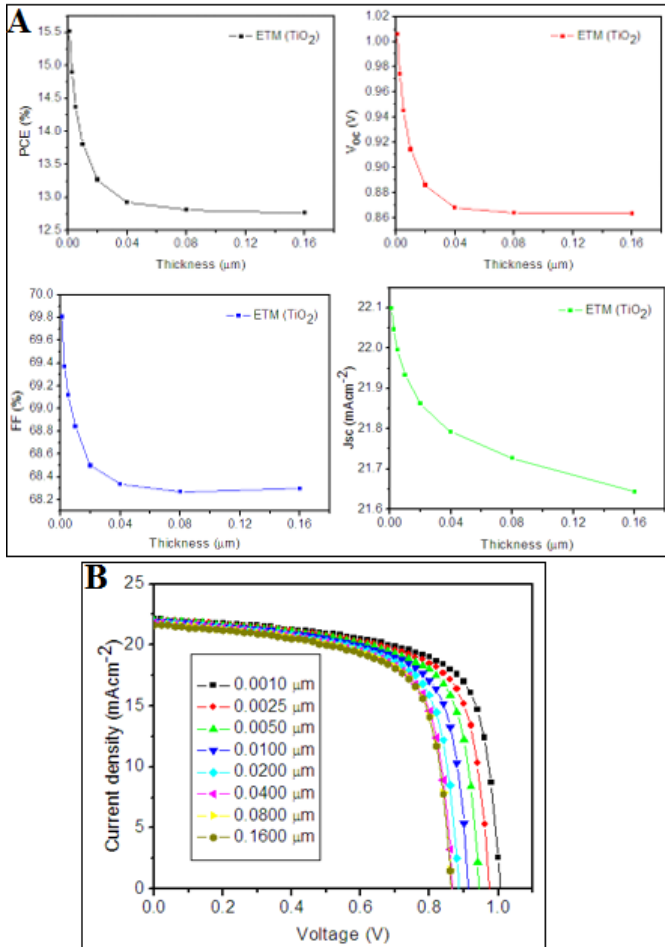


Figure 6: (A) Variation in performance parameters of PSC with thickness of ETM, (B) J–V curves of PSC with different values of thickness of ETM.

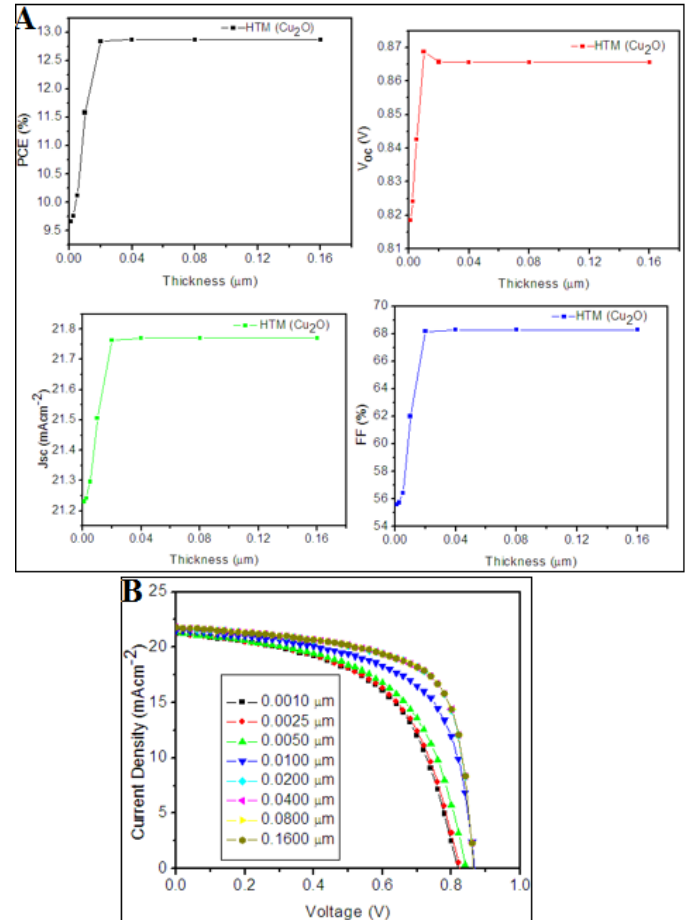


Figure 7: (A) Variation in performance parameters of PSC with thickness of HTM, (B) J–V curves of PSC with different values of thickness of HTM.

3.4. Influence of thickness of absorber layer

There is another parameter, thickness of absorber layer, which affects the performance of solar cell. The influence of thickness

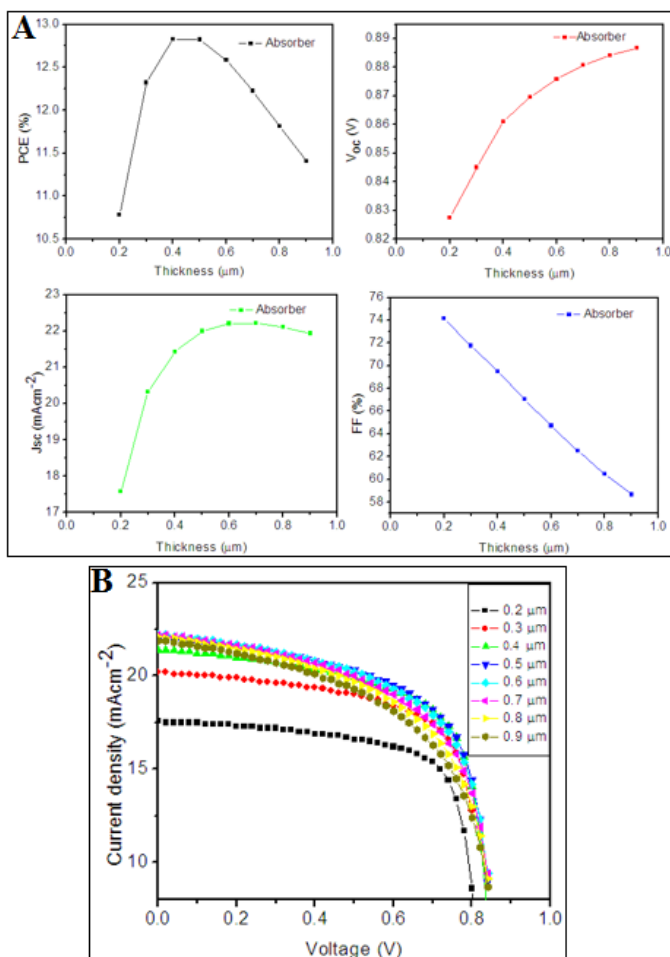


Figure 8: (A) Variation in performance parameters of PSC with thickness of Absorber, (B) J–V curves of PSC with different values of Absorber thickness.

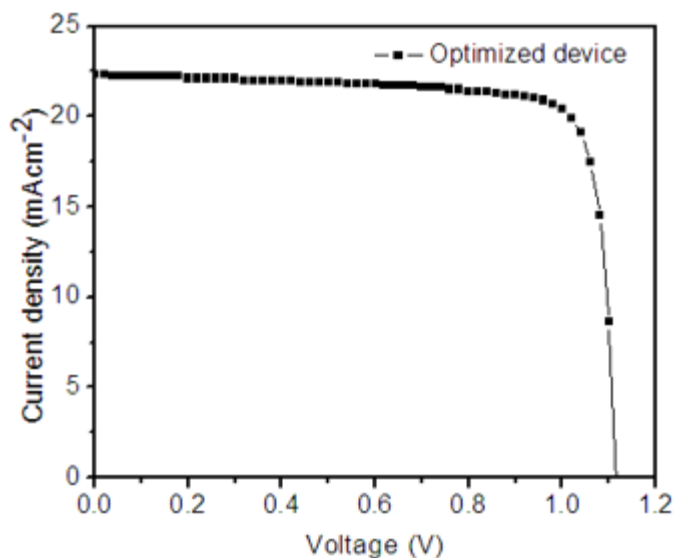


Figure 9: J–V curves of PSC with Optimized parameters.

of absorber on the solar cell parameters; V_{OC} , J_{SC} , FF and PCE is shown in Figure 8(B). PCE is lower when thickness of the layer is too small ($0.2 \mu\text{m}$) due to the poor light absorption. PCE of PSCs increases with the increase of the thickness of the absorber 0.20 to $0.40 \mu\text{m}$ before it starts decreasing. For thickness beyond $0.4 \mu\text{m}$, the collection of photo generated carriers decreased because of charge recombination.

The PCE of the device increases when thickness of the absorber layer increases. PCE decreases when thickness is larger than $0.40 \mu\text{m}$. Considering, the effect of thickness of the absorber, the optimized parameters are PCE of 12.83% . J_{SC} of $21.43 \text{ mA}/\text{cm}^2$, V_{OC} of 0.86 V , and FF of 69.51% , as shown in Table 8. It is evident from literature that pin hole free structure of methyl ammonium lead iodide perovskite can be obtained by using dimethyl sulfoxide (DMSO) and using polyethylene glycol (PEG) also gives a better effects on the surface morphology [18, 43, 44]. By using solvent retarding method (SR), optimal thick and uniform perovskite film can be deposited [45].

3.5. Performance of Optimized parameters

At the end, considering all the factors as doping concentration, electron affinity and thickness, we obtained PCE to be 20.42% with current density of $22.26 \text{ mA}/\text{cm}^2$, voltage of 1.12 V , and fill factor of 82.20% , which shows an improvement of 58.80% , 2.25% , 20.40% and 30.23% in PCE, J_{sc} , FF and V_{oc} over the initial cell. The final optimized parameters and optimised J–V curve are shown in Table 9 and Figure 9 respectively. We compared our simulated results with the experiment work published by other researchers and the related data is summarized in Table 10.

In the literature, the best efficiency of 11.03% has been achieved for PSCs with Cu_2O as HTM. The V_{OC} , FF and J_{SC} still need to be increased to achieve 20.42% efficiency. This could be achieved by further improving the film morphology and crystalline quality of both the absorber and Cu_2O layer. Doping of Cu_2O by replacing either part of Cu or part of O by other element might/can further modify the charge carrier concentration and mobility of HTM.

4. Conclusion

In this work, the lead-based perovskite solar cells with Cu_2O as HTM are studied by one dimensional simulation programme. The results show that optimum doping concentration in the absorber layer gives improved PCE. High values of doping concentration leads to decrease of PCE due to higher recombination rates. To reduce the recombination rates at the interfaces, proper selection is made for the electron affinity of ETM and HTM. By choosing the electron affinity of ETM as 3.7 eV , PCE of PSCs increases from 12.86% to 20.29% , and by choosing the electron affinity of HTM as 3.3 eV , PCE of PSCs increases from 12.86% to 13.11% . With the optimised thickness of $0.001 \mu\text{m}$, for ETM layer, the PCE of the device increases from 12.86% to 15.52% . With the optimised HTM thickness of $0.16 \mu\text{m}$, thus, PCE increases up to 12.87% . The overall PCE, FF, J_{SC} , and V_{OC} , of 20.42% , 82.20% , $22.26 \text{ mA}/\text{cm}^2$,

and 1.12 V respectively were obtained by using all optimised parameters. The results show that Cu_2O as alternate HTM has the potential to be used with $CH_3NH_3PbI_3$ and can replace the spiro-MeOTAD which is costly HTM for perovskite solar cell.

Acknowledgments

We thank the referees for the positive enlightening comments and suggestions, which have greatly helped us in making improvements to this paper. The authors would also like to thank Professor Marc Burgelman, Department of Electronics and Information Systems, University of Gent for the development of the SCAPS software package and for allowing its use.

References

- [1] J. S. Manser, & P. V. Kamat "Band filling with free charge carriers in organometal halide perovskites", *Nature Photonics* **8** (2014) 737.
- [2] H. Chen, F. Ye, W. Tang, J. He, M. Yin, Y. Wang, F. Xie, E. Bi, X. Yang, M. Gratzel, L. Han, "A solvent- and vacuum-free route to large-area perovskite films for efficient solar modules", *Nature* **550** (2017) 92.
- [3] G. Xing, N. Mathews, S. Sun, S. S. Lim, Y. M. Lam, M. Gratzel, S. Mhaisalkar, T. C. Sum, "Long-range balanced electron and hole-transport lengths in organic-inorganic $CH_3NH_3PbI_3$ ", *Science* **342** (2013) 344.
- [4] M. Liu, M. B. Johnston, & H. J. Snaith, "Efficient planar heterojunction perovskite solar cells by vapour deposition", *Nature* **501** (2013) 395.
- [5] Z. Wang, Q. Lin, F. P. Chmiel, N. Sakai, L. M. Herz, H. J. Snaith, "Efficient ambient-air-stable solar cells with 2D-3D heterostructured butylammonium-caesium-formamidinium lead halide perovskites", *Nature Energy* **2** (2017) 9.
- [6] Y. Liu, Z. Yang, D. Cui, X. Ren, J. Sun, X. Liu, J. Zhang, Q. Wei, H. Fan, F. Yu, X. Zhang, C. Zhao, S. Liu, "Two-inch-sized perovskite $CH_3NH_3PbX_3$ (X = Cl, Br, I) crystals: growth and characterization", *Advanced Materials* **27** (2015) 5176.
- [7] D. Yang, Z. Yang, W. Qin, Y. Zhang, S. Liu, C. Li, "Alternating precursor layer deposition for highly stable perovskite films towards efficient solar cells using vacuum deposition", *Journal of Materials Chemistry A* **3** (2015) 9401.
- [8] S. Yakunin, D. N. Dirin, Y. Shynkarenko, V. Morad, I. Cherniukh, O. Nazarenko, D. Kreil, T. Nauser, M. V. Kovalenko, "Detection of gamma photons using solution-grown single crystals of hybrid lead halide perovskites", *Nature Photonics* **10** (2016) 585.
- [9] F. Hao, K. Stoumpos, D. H. Cao, R. P. H. Chang, M. Kanatzidis, "Lead-free solid-state organic-inorganic halide perovskite solar cells", *Nature Photonics* **8** (2014) 489.
- [10] Y. Shao, Z. Xiao, C. Bi, Y. Yuan, & J. Huang, "Origin and elimination of photocurrent hysteresis by fullerene passivation in $CH_3NH_3PbI_3$ planar heterojunction solar cells", *Nature Communications* **5** (2015) 5784.
- [11] H. Wei, Y. Fang, P. Mulligan, W. Chuirazzi, H. Fang, C. Wang, B. R. Ecker, Y. Gao, M. A. Loi, L. Cao, J. Huang, "Sensitive X-ray detectors made of methylammonium lead tribromide perovskite single crystals", *Nature Photonics* **10** (2016) 333.
- [12] I. Chung, B. Lee, J. He, R. P. H. Chang & M. G. Kanatzidis, "All-solid-state dye-sensitized solar cells with high efficiency", *Nature* **485** (2012) 486.
- [13] Y. C. Kim, K. H. Kim, D. Y. Son, D. N. Jeong, J. Y. Seo, Y. S. Choi, I. T. Han, S. Y. Lee, N. G. Park, "Printable organometallic perovskite enables large-area, low-dose X-ray imaging", *Nature* **550** (2017) 87.
- [14] Y. Liu, Y. Zhang, Z. Yang, D. Yang, X. Ren, L. Pang, S. F. Liu, "Thickness- and shape-controlled growth for ultrathin single-crystalline perovskite wafers for mass production of superior photoelectronic devices", *Advanced Materials* **28** (2016) 9204.
- [15] P. Gao M. Gratzel and M. K. Nazeeruddin, "Organohalide lead perovskites for photovoltaic applications", *Energy and Environmental Science* **7** (2014) 2448.
- [16] W.S Yang, B. M. Park, E. H. Jung, N. J. Jeon, Y. C. Kim, D. U. Lee, S. S. Shin, J. Seo, E. K. Kim, J. H. Noh, S. I. Seok, "Iodide management in formamidinium-lead-halide-based perovskite layers for efficient solar cells", *Science* **356** (2017) 1376.
- [17] K. T. Cho, S. Paek, G. Grancini, C. R. Carmona, P. Gao, Y. Lee, M. K. Nazeeruddin, "Highly efficient perovskite solar cells with a compositionally engineered perovskite/hole transporting material interface", *Energy and Environmental Science* **10** (2017) 621.
- [18] S. Z. Haider, H. Anwar and M. Wang, "A comprehensive device modelling of perovskite solar cell with inorganic copper iodide as hole transport material", *Semiconductor Science and Technology* **33** (2018) 12.
- [19] N. Rajamanickam, S. Kumari, V. K. Vendra, B. W. Lavery, J. Spurgeon, T. Druffel, and M.K. Sunkara, "Stable and durable $CH_3NH_3PbI_3$ perovskite solar cells at ambient conditions", *Nanotechnology* **27** (2016) 235404.
- [20] K. G. Lim, H. B. Kim, J. Jeong, H. Kim, J. Y. Kim, and T. W. Lee, "Boosting the power conversion efficiency of perovskite solar cells using self-organized polymeric hole extraction layers with high work function", *Advanced Materials* **26** (2014) 6461.
- [21] D. Wang, M. Wright, N. K. Elumalai, and A. Uddin, "Stability of perovskite solar cells", *Solar Energy Materials and Solar Cells* **147** (2016) 255.
- [22] W. Li, H. Dong, L. Wang, N. Li, X. Guo, J. Li, Y. Qiu, "Montmorillonite as bifunctional buffer layer material for hybrid perovskite solar cells with protection from corrosion and retarding recombination", *Journal of Materials Chemistry A* **2** (2014) 13587.
- [23] R.S. Sanchez, and E. Mas-Marza, "Light-induced effects on Spiro-OMeTAD films and hybrid lead halide perovskite solar cells", *Solar Energy Materials Solar Cells* **158** (2016) 189.
- [24] X. Zhao, and N-G. Park, "Stability issues on perovskite solar cells", *Photonics* **2** (2015) 1139.
- [25] W. Chen, Y. Wu, Y. Yue, J. Liu, W. Zhang, X. Yang, H. Chen, E. Bi, I. Ashraf, M. Gratzel, L. Han, "Efficient and stable large-area perovskite solar cells with inorganic charge extraction layers", *Science* **350** (2015) 944.
- [26] Y. Hou, X. Du, S. Scheiner, D. P. McMeekin, Z. Wang, N. Li, M. S. Killian, H. Chen, M. Richter, I. Levchuk, N. Schrenker, E. Spiecker, T. Stubhan, N. A. Luechinger, A. Hirsch, P. Schmuki, H. P. Steinruck, R. H. Fink, M. Halik, H. J. Snaith, C. J. Brabec, "A generic interface to reduce the efficiency-stability-cost gap of perovskite solar cells", *Science* **358** (2017) 1192.
- [27] G. Grancini, C. Roldan-Carmona, I. Zimmermann, E. Mosconi, X. Lee, D. Martineau, S. Narbey, F. Oswald, F. De Angelis, M. Gratzel, M. K. Nazeeruddin, "One-year stable perovskite solar cells by 2D/3D interface engineering", *Nature Communications* **8** (2017) 15684.
- [28] A. Mei, X. Li, L. Liu, Z. Ku, T. Liu, Y. Rong, M. Xu, M. Hu, J. Chen, Y. Yang, M. Gratzel, H. Han, "A hole-conductor-free fully printable mesoscopic perovskite solar cell with high stability", *Science* **345** (2014) 295.
- [29] N. Arora, M. I. Dar, A. Hinderhofer, N. Pellet, F. Schreiber, S. M. Zaakeeruddin, M. Gratzel, "Perovskite solar cells with $CuSCN$ hole extraction layers yield stabilized efficiencies greater than 20 %". *Science* **358** (2017) 768.
- [30] W. Yu, F. Li, H. Wang, E. Alarousu, Y. Chen, B. Lin, L. Wang, M. N. Hedhili, Y. Li, K. Wu, X. Wang, O. F. Mohammed and T. Wu, "Ultrathin Cu_2O as an efficient inorganic hole transporting material for perovskite solar cells", *Nanoscale* **8** (2016) 6173.
- [31] Y.J. Chen, M.H. Li, J.C.A. Huang, & P. Chen, " Cu/Cu_2O nanocomposite films as a p-type modified layer for efficient perovskite solar cells", *Scientific Reports* **8** (2018) 7646.
- [32] R. Wei, "Modelling of Perovskite Solar Cells", M.Sc Degree Thesis, Queensland University of Technology 2018.
- [33] M. I. Hossain, F. H. Alharbi, and N. Tabet, "Copper oxide as inorganic hole transport material for lead halide perovskite based solar cells", *Solar Energy* **120** (2015) 370.
- [34] K. Tan, P. Lin, G. Wang, Y. Liu, Z. Xu, and Y. Lin, "Controllable design of solid-state perovskite solar cells by SCAPS device simulation", *Solid State Electron* **126** (2016) 75.
- [35] M. Amalina, and M. Rusop. "Morphological, electrical and optical properties of γ -copper (I) iodide thin films by mist atomization technique", *World Journal of Engineering* **9** (2012) 251.
- [36] U. Mandadapu, S. V. Vedanayakam, and K. Thyagarajan, "Simulation and analysis of lead based perovskite solar cell using SCAPS-1D", *Indian*

- Journal of Science Technology **10** (2017) 1.
- [37] K. G. Lim, S. Ahn, H. Kim, M. R. Choi, D. H. Huh, and T. W. Lee, “Self-doped conducting polymer as a hole-extraction layer in organic–inorganic hybrid perovskite solar cells”, *Advanced Materials Interfaces* **3** (2016) 1500678.
- [38] Q. Wang, Y. Shao, H. Xie, L. Lyu, X. Liu, Y. Gao, and J. Huang, “Qualifying composition dependent p and n self-doping in $CH_3NH_3PbI_3$ ”, *Applied Physics Letters* **105** (2014) 163508.
- [39] L. A. Frolova, N. N. Dremova, and P. A. Troshin, “The chemical origin of the p-type and n-type doping effects in the hybrid methylammonium–lead iodide ($MAPbI_3$) perovskite solar cells”, *Chemical Communication* **51** (2015) 14917.
- [40] C. S. Jiang, M. Yang, Y. Zhou, B. To, S. U. Nanaakkara, J. M. Luther, W. Zhou, J. J. Berry, J. V. de Lagemaat, N. P. Padture, K. Zhu, M. M. Al-jassim, “Carrier separation and transport in perovskite solar cells studied by nanometre-scale profiling of electrical potential”, *Nature Communications* **6** (2015) 8397.
- [41] U. Thakur, R. Kisslinger, and K. Shankar, “One-dimensional electron transport layers for perovskite solar cells”, *Nanomaterials* **7** (2017) 1.
- [42] K. G. Lim, S. Ahn, Y. H. Kim, Y. Qi, and T. W. Lee, “Universal energy level tailoring of self-organized hole extraction layers in organic solar cells and organic–inorganic hybrid perovskite solar cells”, *Energy and Environmental Science* **9** (2016) 932.
- [43] N. J. Jeon, J. H. Noh, Y. C. Kim, W. S. Yang, S. Ryu and S. Seok, “Solvent engineering for high-performance inorganic–organic hybrid perovskite solar cells”, *Nature Materials* **13** (2014) 897.
- [44] M. I. Ahmed, A. Habib and S. S. Javid, “Perovskite solar cells: potentials, challenges, and opportunities”, *International Journal of Photoenergy* **2015** (2014) 1.
- [45] Z. Yuan, Y. Yang, Z. Wu, S. Bai, W. Xu, T. Song, X. Gao, F. Gao, and B. Sun, “Approximately 800 nm thick inhole-free perovskite films via facile solvent retarding process for efficient planar solar cells”, *ACS Applied Materials Interfaces* **8** (2016) 34446.